AGU PUBLICATIONS

Geochemistry, Geophysics, Geosystems

RESEARCH ARTICLE
10.1002/2016GC006282

Key Points:
- Electrical conductivity of eclogite decreased with increasing pressure, and the activation volume and activation energy were calculated
- Electrical conductivity of eclogite increased with oxygen fugacity, and the hopping of small polarons is the dominant conduction mechanism
- The results for various redox conditions cannot explain the high anomalies in conductivity under Dabie-Sulu UHPM belt of eastern China

Supporting Information:
- Supporting Information S1
- Supporting Information S2

Correspondence to:
L. Dai,
dailidong@vip.gyig.ac.cn

Citation:
Dai, L., H. Hu, H. Li, L. Wu, K. Hui, J. Jiang, and W. Sun (2016), Influence of temperature, pressure, and oxygen fugacity on the electrical conductivity of dry eclogite, and geophysical implications, *Geochem. Geophys. Geosyst.*, *17*, 2394–2407, doi:10.1002/2016GC006282.

Received 29 JAN 2016
Accepted 26 MAY 2016
Accepted article online 30 MAY 2016
Published online 24 JUN 2016

Influence of temperature, pressure, and oxygen fugacity on the electrical conductivity of dry eclogite, and geophysical implications

Lidong Dai[1], Haiying Hu[1], Heping Li[1], Lei Wu[1], Keshi Hui[1], Jianjun Jiang[1,2], and Wenqing Sun[1,2]

[1]Key Laboratory of High-temperature and High-pressure Study of the Earth's Interior, Institute of Geochemistry, Chinese Academy of Sciences, Guiyang, China, [2]University of Chinese Academy of Sciences, Beijing, China

Abstract The electrical conductivity of eclogite was measured at temperatures of 873–1173 K and pressures of 1.0–3.0 GPa within a frequency range of 0.1–10^6 Hz using a YJ-3000t multianvil press and Solartron-1260 impedance/gain-phase analyzer. Three solid-state oxygen buffers (Cu + CuO, Ni + NiO, and Mo + MoO_2) were employed to control the oxygen fugacity. Experimental results indicate that the electrical conductivity of the samples tended to increase with increasing temperature, conforming to an Arrhenius relation. Under the control of a Cu + CuO oxygen buffer, the electrical conductivity of the eclogite decreased with a rise in pressure, and its corresponding activation volume and activation energy at atmospheric pressure were calculated as -2.51 ± 0.29 cm^3/mole and 0.86 ± 0.12 eV, respectively. At 2.0 GPa, the electrical conductivity of the eclogite increased with increasing oxygen fugacity, and the preexponential factor increased while the activation enthalpy decreased. The observed positive exponential factor for the dependence of electrical conductivity on oxygen fugacity, as well as the negative activation volume, confirm that the hopping of small polarons is the dominant conduction mechanism in eclogite at high temperatures and pressures. Our results suggest that the electrical conductivity of dry eclogite under various redox conditions cannot explain the high anomalies in conductivity under stable midlower continental crust and under the Dabie-Sulu ultrahigh-pressure metamorphic belt of eastern China.

1. Introduction

Oxygen fugacity, just like temperature and pressure, is one of the crucial factors affecting the results in high-pressure experimental studies of the electrical properties of minerals and rocks involving multivalent elements. Oxygen fugacity plays a substantial role in many of the physical properties of minerals, such as electrical conductivity, grain-growth kinetics, the Seebeck coefficient, the diffusion coefficient, and phase stability [*Roberts and Tyburczy*, 1993; *Roberts and Duba*, 1995; *Du Frane et al*., 2005; *Nishihara et al*., 2008; *Karato*, 2013, 2015; *Burnham and Berry*, 2014; *Knipping et al*., 2015]. Specially, Gaillard recently points out that oxygen fugacity has a remarkable influence on many geochemical processes such as the subduction-related magmatic crystallization and differentiation, iron depletion and element partitioning [*Gaillard et al*., 2015].

Results on the field magnetotelluric surveys have revealed that the anomalous high electrical conductivity zone (conductivities $\geq 10^{-1}$ S/m) in the world-famous Dabie-Sulu ultra-high pressure metamorphic belts of eastern China exists at depths of 12–21 km [*Hu et al*., 2000; *Xiao et al*., 2007; *He et al*., 2009]. As a representative high-temperature and high-pressure metamorphic rock, eclogite forms as a result of high-pressure metamorphism of gabbro or basalt at depths of 50–300 km during subduction and the consequential continental collision of blocks. It would be usual for eclogite to exist at a depth of ~100 km in the deep interior of the Earth, and the typical eclogite would be composed of approximately equal volume fractions of garnet and omphacite [*Zheng et al*., 2003; *Tang et al*., 2007]. Therefore, there have been many studies on the electrical conductivity of natural eclogite [e.g., *Laštovičková and Parchomenko*, 1976; *Čermák and Laštovičková*, 1987; *Bagdassarov et al*., 2011]. Measurements of the dielectric constant and the electrical conductivity for both direct and single-frequency alternating currents in eight natural eclogites from the Bohemian Massif were conducted by *Laštovičková and Parchomenko* [1976] under pressures up to 2.0 GPa, temperatures of 473–1173 K, and for different mineralogical compositions. The authors found that the

Table 1. Results of Electron Microprobe (EPMA) Analyses of the Main Constituent Minerals in Eclogite, and X-Ray Fluorescence (XRF) Analyses of the Eclogite Whole-Rock

Oxides (wt%)	EPMA for Garnet[a]	EPMA for Omphacite[a]	XRF for Whole Rock[b]
SiO_2	38.01	56.74	50.39
TiO_2	0.03	0.09	0.71
Cr_2O_3	0.16	0.95	–
Al_2O_3	20.66	10.30	14.67
FeO	31.66	4.36	8.02
MnO	0.91	0.03	0.08
CaO	6.88	13.84	10.54
MgO	1.86	7.49	5.29
K_2O	0.01	0.09	0.06
Na_2O	0.01	7.02	5.68
P_2O_5	–	–	0.65
LOI[c]	–	–	3.74
Total	100.20	100.90	99.83
Mineral compositions (volume %)	~41% garnet	~58% omphacite	<1% hydrous accessory minerals (e.g., amphibole, mica, etc.)

[a]All Fe from the electron microprobe (EPMA) analyses is expressed as FeO.
[b]All Fe_2O_3 from the X-ray fluorescence (XRF) analyses is expressed as FeO. [c]LOI denotes the loss on ignition.

electrical conductivity of eclogite tended to increase with increasing content of symplectite (such as intergrowths of amphibole-plagioclase or diopside-plagioclase). Subsequently, *Čermák and Laštovičková* [1987] measured the electrical conductivity of eclogite from upper Saxony at room pressure, at temperatures of 473–1473 K, and with an argon atmosphere at a partial oxygen pressure of $\sim 10^{-1}$ Pa, and they compared their results with magnetotelluric data for the crust and upper mantle. *Bagdassarov et al.* [2011] used a piston-cylinder high-pressure apparatus to investigate the electrical conductivity of the At-Bashi eclogite (from the lithosphere of the Tien Shan) at 2.5 GPa, 623–1423 K, and with a Mo + MoO_2 oxygen buffer. However, all these earlier studies of the electrical conductivity of eclogite were performed at a defined pressure, and the effects of pressure and oxygen fugacity on the electrical conductivity of eclogite remain unclear.

In the present study, we have measured the electrical conductivity of eclogite at temperatures of 873–1173 K, pressures of 1.0–3.0 GPa, and with the use of three solid buffers to control oxygen fugacity, namely Cu + CuO, Ni + NiO, and Mo + MoO_2. Our results, as outlined in this paper, allow us to discuss in detail the influence of temperature, pressure, and oxygen fugacity on the electrical conductivity of eclogite.

2. Experimental Procedures

2.1. Sample Characterization

The natural eclogite samples used in this study were collected from the Dabie-Sulu ultrahigh-pressure metamorphic belt of eastern China. This belt represents the collisional suture zone between the Sino-Korean and Yangtze cratons. The NNE trending Tan-Lu Fault divides the terrane into two orogenic belts: the Dabie belt to the west and the Sulu belt to the east. The eclogite samples are fresh, unoxidized, and free of fractures, and there was no evidence of alteration of the rock, either before or after the conductivity experiments. The samples are coarse-grained with a crystalloblastic texture (~250 μm grain size). The chemical compositions of the samples were determined using a PANalytical Axios-advance (Axios PW4400) X-ray fluorescence spectrometer (XRF) and an electron-microprobe analyzer (EPMA-1600) at the State Key Laboratory of Ore-Deposit Geochemistry in the Institute of Geochemistry, Chinese Academy of Sciences, Guiyang, China; the analytical results are given in Table 1. By virtue of the mass balance calculation for the whole rock composition, the sample contains ~41% garnet, ~58% omphacite and <1% hydrous accessory minerals (e.g., amphibole, mica, et al.). The average garnet composition from electronic microprobe analysis is ~$Alm_{70.7}Grs_{19.8}Py_{7.4}Sps_{2.1}$. The samples were cut and polished with an ultrasonic drill and diamond slicer into cylinders 6.0 mm long and 6.0 mm diameter before they were cleaned in solutions containing deionized distilled water, alcohol, and acetone. The samples were then heated at 423 K in a vacuum drying oven for 96 hrs to remove the water adsorbed on the surfaces of the samples.

The mineral content, modal variations, and texture of the eclogite were investigated with a polarizing microscope before and after the electrical conductivity work, as shown in Figures 1a and 1b. Two representative back-scattered electron images are shown in Figures 1c and 1d, which endures a feeble slightly retrogressive metamorphism and accompanies during the measurement of electrical conductivity process at

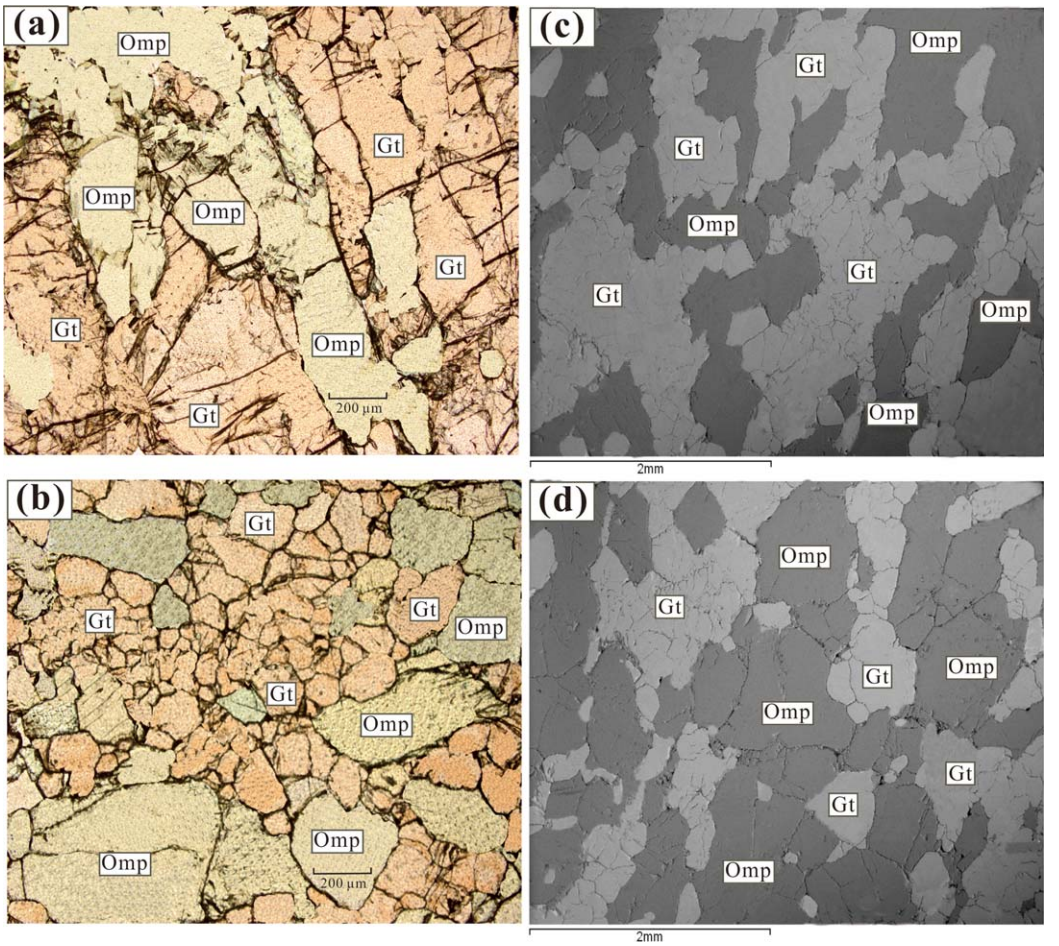

Figure 1. Representative images of the Dabie-Sulu eclogite. (a and b) Photomicrographs (plane-polarized reflected) taken light before and after electrical conductivity measurements, respectively. (c and d) Back-scattered electron images using a scanning electron microscope. Abbreviations are *Gt* garnet and *Omp* omphacite.

high temperature and high pressure, and however it cannot result in the variation of mineralogical assemblage. Samples recovered after the electrical conductivity work did not contain any glass or quenched crystals, and it is therefore assumed that the eclogite remained entirely crystalline during the *in situ* electrical conductivity measurements.

To determine the water content in the each constituent minerals of garnet and omphacite for eclogite, a Fourier transform infrared analysis (FT-IR) with a wavenumber range of 3000–4000 cm^{-1} was conducted both before and after the electrical conductivity measurements in the German Brucker company of Peking division. The FT-IR absorption spectra for the samples are displayed in Figure 2. Based on the representative hydrogen-related bands in the range of 3000–3750 cm^{-1}, the water content in the sample was worked out using the formula proposed by *Paterson* [1982].

The water contents for garnet before and after conductivity measurements are less than ~5 $H/10^6$ Si and ~7 $H/10^6$ Si, respectively. The water contents for omphacite before and after conductivity measurements are less than ~4 $H/10^6$ Si and ~9 $H/10^6$ Si, respectively. And thus, we call it as really "dry" eclogite. The variation of water content during the electrical conductivity measurements of dry sample is not more than 15%.

2.2. High-Pressure Cell and Impedance Measurements

The *in situ* electrical conductivity measurements on the eclogite at high temperatures and pressures were performed with a Solartron-1260 impedance/gain-phase analyzer (Schlumberger) and YJ-3000t multianvil apparatus at the Key Laboratory of High-Temperature and High-Pressure Study of the Earth's Interior,

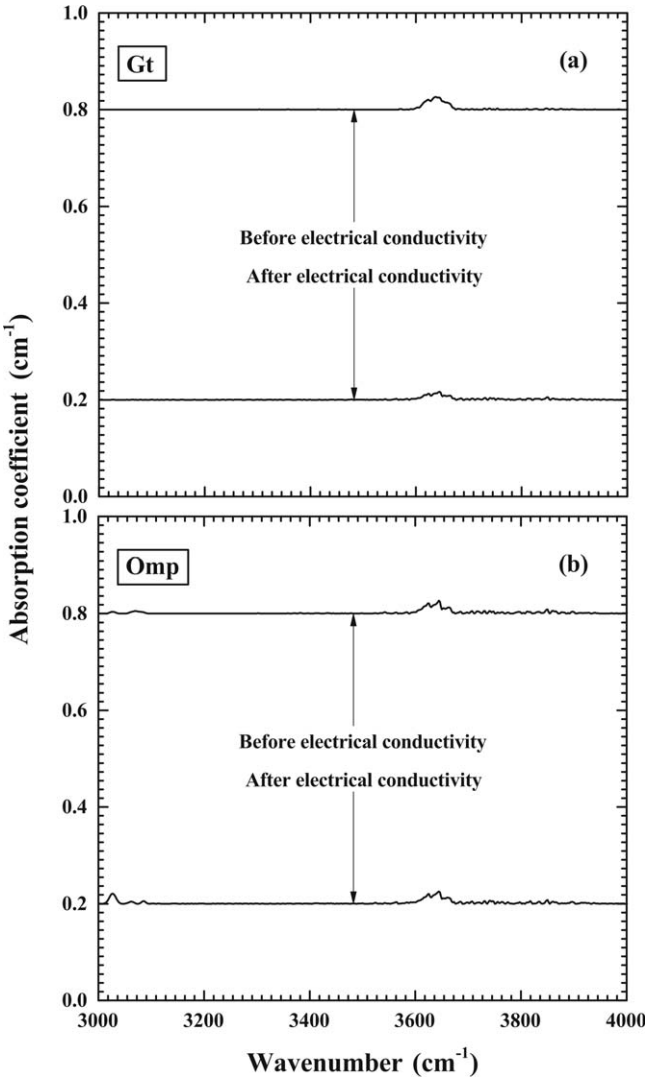

Figure 2. The unpolarized FT-IR spectra of the dominant phases in the studied eclogite: garnet (*Gt*) and omphacite (*Opm*) before and after electrical conductivity measurements.

Institute of Geochemistry, Chinese Academy of Sciences, Guiyang, China. Detailed descriptions of the high-pressure equipment and the experimental procedures can be found in *Dai et al*. [2008] and *Hu et al*. [2011].

High pressures were generated in the YJ-3000t multianvil press using six symmetric cubic tungsten carbide anvils with a total surface area of 23.4 mm^2. A cross-sectional image of the high-pressure cell assembly, recovered after the electrical conductivity work, is given in Figure 3. To avoid the influence of absorbed water on the conductivity measurements, all the equipment, including the cubic pressure medium of pyrophyllite, the magnesium oxide tubes, and the alumina insulation sleeves, was baked at 1073 K for 5 hrs in a muffle furnace prior to sample assembly. The cylindrical eclogite samples with a diameter of 6.0 mm were placed between the Al_2O_3 insulation sleeves and the two symmetrically sandwiched metal electrodes. A metal Faraday shielding case made of 0.025 mm metal foil, and connected to the Earth line by the NiAl Earth line, was installed between the MgO tubes and the Al_2O_3 insulation sleeves, and this efficiently reduced the temperature gradient within the sample cell and the signal disturbance of impedance measurements. The experimental temperatures were monitored with a NiCr-NiAl thermocouple. The oxygen fugacity was monitored and adjusted by changing the types of metal (Cu, Ni, and Mo) in the two electrodes and their correspondent shielding cases; the thicknesses of each electrodes was 0.5 mm. To assess the validity of the oxygen buffer, the interface between the electrode and sample, recovered after the electrical conductivity measurements, was

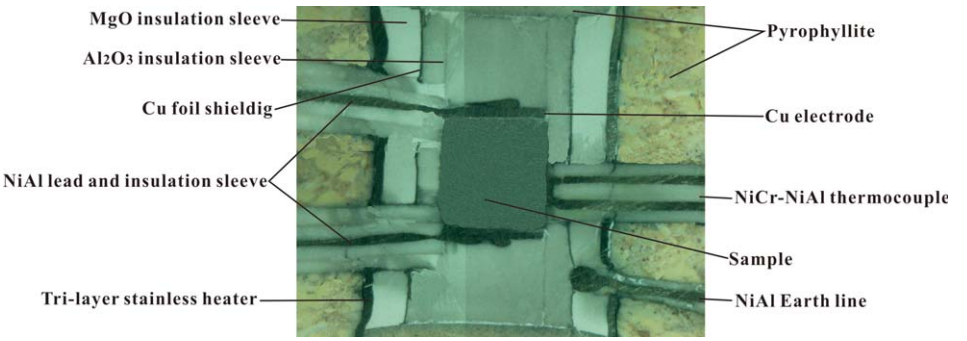

Figure 3. A photomicrograph (plane-polarized reflected) taken light from the sample assembly after conductivity measurement.

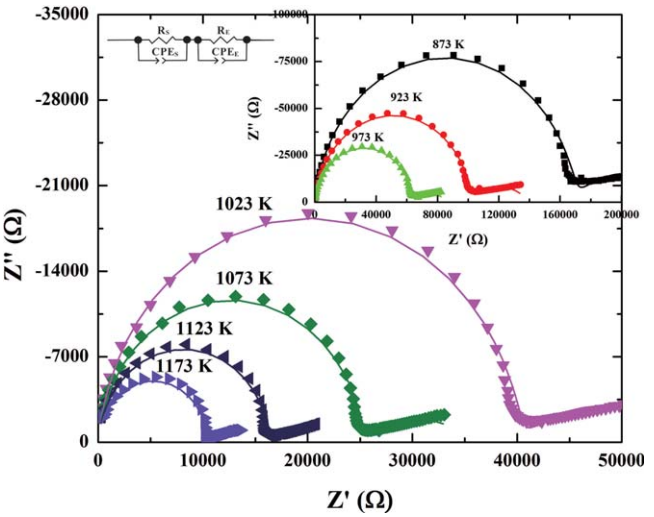

Figure 4. Nyquist plane impedance of eclogite at frequencies from 10^{-1} to 10^{6} Hz (right to left), obtained under conditions of 3.0 GPa, 873–1173 K, and a Cu + CuO solid buffer. Z' and Z'' are the real and imaginary parts of complex impedance, respectively. The equivalent circuit that is composed of the series connection of R_S-CPE_S and R_E-CPE_E (R_S and CPE_S represent the resistance and the constant-phase element of the bulk impedance for the sample, respectively; R_E and CPE_E represent the resistance and the constant phase element from the polarization effect of the sample-electrode interface, respectively) is selected to model the impedance semicircles.

examined under a scanning electron microscope to verify the coexistence of metal and its corresponding metallic oxide (e.g., Cu + CuO, Ni + NiO, and Mo + MoO_2), and we were successful in verifying this. Measurement errors from the pressure (P) and temperature (T) gradients were indicated as less than 0.2 GPa and 10 K, respectively. The uncertainty of electrical conductivity was estimated to be less than 5% and mainly due to the estimations of geometric factor of the sample and the equilibrium circuit of data fitting for the semicircular arc of impedance spectra.

During the experiments, pressures were increased slowly at a rate of 1.0 GPa/h to the desired value. Then, under constant pressure conditions the temperature was increased gradually at a rate of 120 K/h to the designated preset value by steps of 50 K, and the impedance spectroscopy measurements were performed at various temperatures and oxygen fugacities. After the temperature reached each preset value under conditions of constant pressure and a specific oxygen fugacity, complex impedance spectra were collected using the ZPlot software of the Solartron-1260 impedance/gain-phase analyzer within a frequency range of 10^{-1} to 10^{6} Hz and at 1.0 V signal voltage. To check the conductivity hysteresis effect, the impedance spectra of samples were measured during both heating and cooling cycles. One representative equivalent circuit, made up of an appropriate series of parallel constant phase elements (CPE) and a resistor, was selected to fit the impedance semicircular arcs within the high- and low-frequency ranges. Only high-frequency impedance semicircles were used to calculate the electrical conductivities of samples. For each experiment in the first heating cycle, the sample was heated up to 1123 K under a given pressure and oxygen fugacity conditions, and electrical conductivity measurements were recorded continuously enough long elapsed time so as to attain the self-buffered for solid buffer and the constant equilibrium redox state (the redox re-equilibration). Then, we continued to heat sample till the maximum designated temperature point of 1173 K and reproduced above-mentioned steps. Lastly, after the first heating cycle, each conductivity data point for other cycles was acquired at the equilibrium redox states under controlled different P, T and fO_2 conditions so as to reach the previously mentioned redox "reequilibration" effect of controlled oxygen fugacity [*Huebner and Voigt*, 1988; *Wanamaker*, 1994; *Gaillard*, 2004; *Pommier et al.*, 2010].

The experimental results indicate that the conductivity data from the first heating cycle deviated in an obvious way from the other cycles, but that the other three cycles (i.e., the first cooling, second heating, and second cooling cycles) generally produced reproducible data. The possible reason for the difference in the electrical conductivity of eclogite in the first heating and other cycles is due to the comprehensive impacts from the redox reequilibrium effect and the loss of volatiles among the first heating cycle. Therefore, for each experiment a set of reproducible data that did not include the first heating cycle was chosen for the subsequent data fitting and analysis.

3. Results

In the experiments, we obtained the results for electrical conductivities of eclogite under pressures of 1.0–3.0 GPa, temperatures of 873–1173 K, and with Cu + CuO controlled oxygen fugacity, and also at 2.0 GPa and 873–1173 K with three different solid buffers (Cu + CuO, Ni + NiO, and Mo + MoO_2).

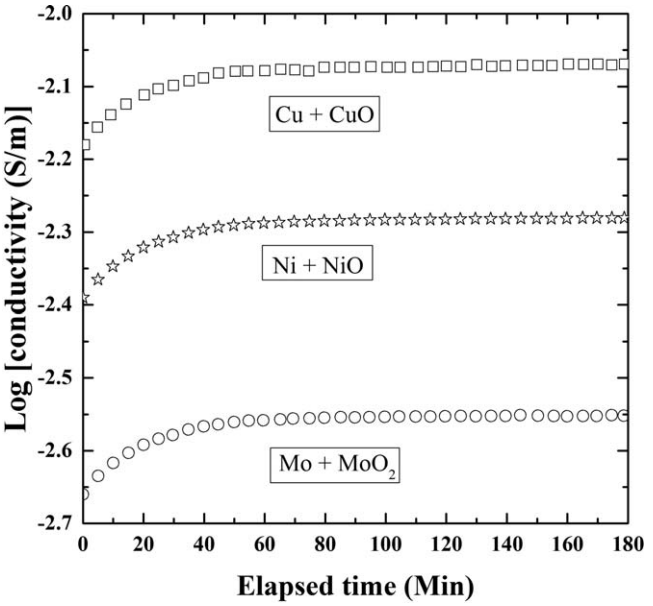

Figure 5. A functional relationship between the electrical conductivity of eclogite and the elapsed time under conditions of 2.0 GPa, 1123 K and three different solid buffers (e.g., Cu + CuO, Ni + NiO, and Mo + MoO_2).

Typical complex impedance spectra of eclogite at 3.0 GPa and 873–1173 K, and with Cu + CuO redox conditions, are shown in Figure 4. The results obtained under other conditions resemble these illustrated as follows. Each result displays one approximately semicircular arc at high frequencies (>200 Hz) and another small tail at low frequencies (200–0.1 Hz), and these respectively represent the bulk electrical properties of the sample from which we determined the electrical conductivity of the eclogite and the polarization effect of the sample-electrode interface. As pointed out by *Nover et al.* [1992] and *Roberts and Tyburczy* [1991, 1994], different conduction processes with various characteristic relaxation time constants for the complex plane can be used to determine each conduction process. To make precise fits and acquire the conductivity results from the impedance spectra data, we chose one nonideal constant phase element (CPE) instead of an ordinary capacitance to fit the impedance semicircular arc for the eclogite. The equivalent circuit that is composed of the series connection of R_S-CPE_S and R_E-CPE_E (R_S and CPE_S represent the resistance and constant-phase element of the bulk impedance for the sample, respectively; R_E and CPE_E represent the resistance and constant phase element from the polarization effect of the sample-electrode interface, respectively) was selected to model the impedance semicircles and obtain the bulk resistance for the eclogite samples [*Roberts*, 2002]. The electrical conductivity of the sample is then calculated as

$$\sigma = \frac{G}{R} = \frac{L}{RS} \tag{1}$$

where σ is the electrical conductivity (S/m), G is the geometric factor (m^{-1}), R is the resistance (Ω), L is the length of the sample (m), and S is the cross-sectional area of the electrode (m^2). The electrical conductivity of the eclogite and the temperature were found to satisfy the Arrhenius relation,

$$\sigma = \sigma_0 \times f_{O_2}^i \times \exp\left(-\frac{\Delta H}{kT}\right) = \sigma_0 \times f_{O_2}^i \times \exp\left(-\frac{\Delta U + P \times \Delta V}{kT}\right) \tag{2}$$

where σ_0 is the preexponential factor (S/m), ΔH is the activation enthalpy (eV), ΔU is the activation energy (eV), ΔV is the activation volume (cm^3/mole), P is the pressure (GPa), T is the absolute temperature (K), fO_2 is the oxygen fugacity (bar), k is the Boltzmann constant (eV/K) and i is a constant.

In order to check the redox re-equilibration effect of oxygen buffer, a functional relationship between the electrical conductivity of eclogite and the elapsed time under conditions of 2.0 GPa, 1123 K and three different solid buffers (e.g., Cu + CuO, Ni + NiO, and Mo + MoO_2) is depicted in Figure 5. The electrical conductivities for different heating/cooling cycles at a pressure of 3.0 GPa and with the Cu + CuO solid buffer are shown in Figure 6. The influence of pressure on the electrical conductivity of the eclogite in the temperature range 873–1173 K and with the Cu + CuO solid buffer is illustrated in Figure 7, and the fitted parameters of the Arrhenius relation are listed in Table 2. Figure 8 shows the relationship between electrical conductivity and oxygen fugacity at 2.0 GPa over a broad temperature range of 873 to 1173 K, and with three different oxygen buffers (Cu + CuO, Ni + NiO, and Mo + MoO_2). On the basis of the dependence of electrical conductivity on oxygen fugacity (Figure 8), we were able to fit the exponential factor (i) for the electrical conductivity of eclogite, along with the oxygen fugacity at each corresponding temperature, for a pressure of 2.0 GPa (Table 3).

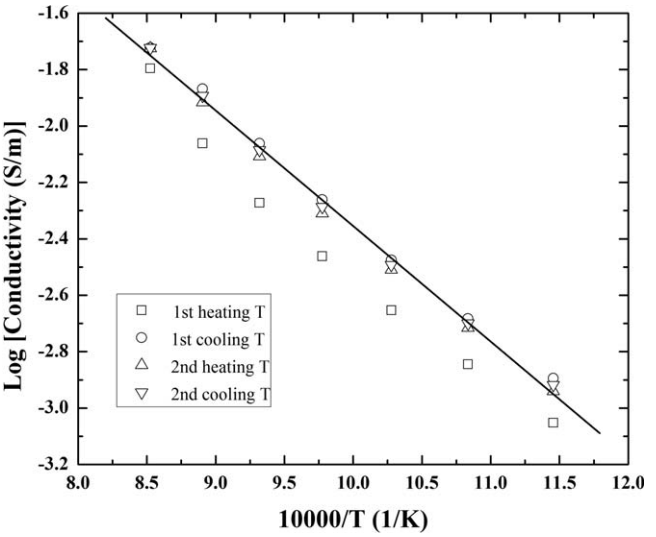

Figure 6. Logarithm of electrical conductivity versus the reciprocal of temperature for eclogite in different heating/cooling cycles at 3.0 GPa and with a Cu + CuO solid oxygen buffer. Data for the first heating cycle were excluded during the data fitting and analysis.

4. Discussion

4.1. Influence of Pressure on Electrical Conductivity

Under the control of a Cu + CuO oxygen buffer, the electrical conductivity of the sample decreased as pressures rose, the activation enthalpy (ΔH) slightly decreased from 0.84 eV to 0.79 eV, and the logarithmic preexponential factor ($\log \sigma_0$) also decreased from 1.83 to 1.43. Although previous researchers have examined the electrical conductivity of the dominant minerals present in eclogite (garnet and clinopyroxene) [*Huebner and Voigt*, 1988; *Romano et al*., 2006; *Dai et al*., 2012], there are no systematic data available for the effects of pressure on the electrical conductivity of eclogite. According to equation (2) and Table 2, the activation energy at atmospheric pressure and the activation volume of the charge carriers can be calculated to be 0.86 ± 0.12 eV and -2.51 ± 0.29 cm^3/mole, respectively, and a linear relationship between $\log \sigma$ and the reciprocal of temperature at room pressure can also be extrapolated from Figure 7. A negative activation volume (ΔV) can be explained by the elastic constants, a strain energy model of defect energy ($G* \propto C\Omega$, where C is the elastic constant of a defect region and Ω is the volume of a defect) [*Keyes*, 1963], the Nernst-Einstein relation, $\sigma = \frac{1}{RT}\sum f_i D_i c_i q_i^2$ (here, f_i is the formation factor for the i-th species, q is the electrical charge of the polarized species, D is the diffusion coefficient, c_i is the concentration of the i-th species, T is the absolute temperature, and R is a gas constant), and a model of diffusion where the preexponential factor is a function of $a^2\nu$ (here, a denotes a lattice constant and ν denotes the vibrational frequency) [*Anderson*, 1989], and thus we obtain

$$\frac{\partial \text{Log } \sigma_0}{\partial P} = \frac{1}{2K}\left(\frac{\partial \text{Log } C}{\partial \text{Log } \rho} - \frac{1}{3}\right) \quad (3)$$

$$\frac{\partial \text{Log } G*}{\partial P} = \frac{V}{G*} = \frac{1}{K}\left(\frac{\partial \text{Log } C}{\partial \text{Log } \rho} - 1\right) \quad (4)$$

where ρ is the density. It is clear that if the derivative for the elastic constant of a defect region on the density $\left(\frac{\partial \text{Log } C}{\partial \text{Log } \rho}\right)$ is less than one, then the derivative for the preexponential factor on the pressure $\left(\frac{\partial \text{Log } \sigma_0}{\partial P}\right)$ and the parameters for the activation volume (ΔV) are negative. Our experimental results, which show the small negative effects of pressure, are similar to those obtained for other materials such as anhydrous single crystals of olivine, orthopyroxene, garnet, and perovskite-magnesiowustite assemblages [*Goddat et al*., 1999; *Xu et al*., 2000;

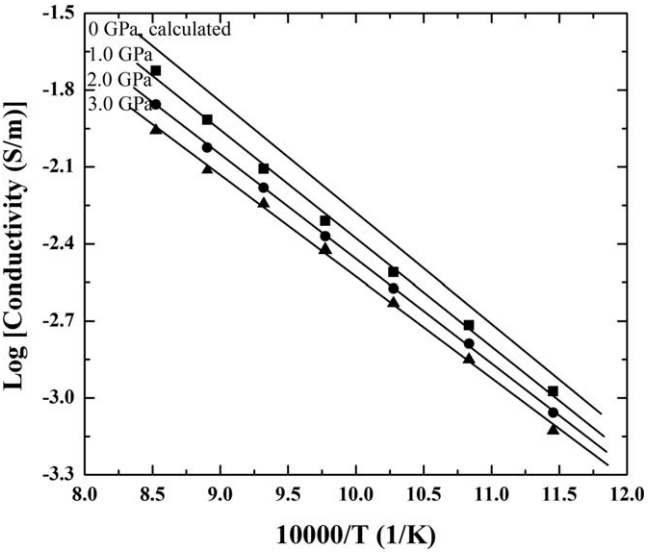

Figure 7. Influence of pressure on the electrical conductivity of eclogite in the temperature range of 873–1173 K and with a Cu + CuO solid oxygen buffer.

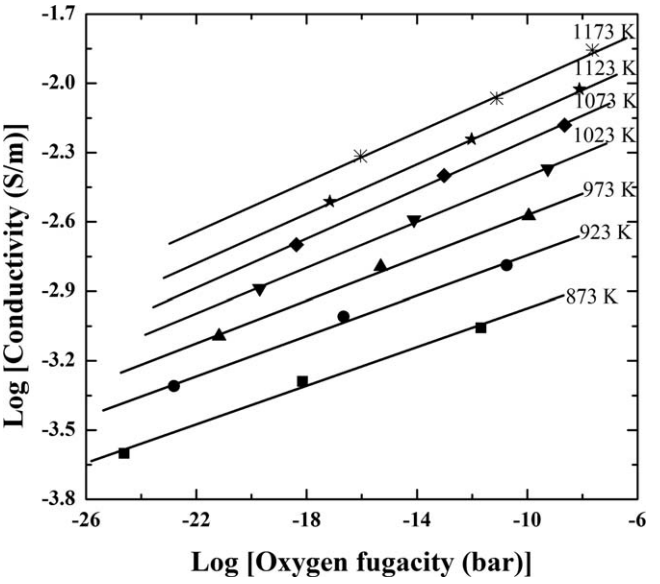

Figure 8. Influence of oxygen fugacity on the electrical conductivity of eclogite under conditions of 2.0 GPa, 873–1173 K, three solid oxygen buffers (Cu + CuO, Ni + NiO, and Mo + MoO_2), and using nonlinear global fitting of the data.

Dai et al., 2005; *Dai and Karato*, 2009a]. Moreover, we note that the reduction in the electrical conductivity of eclogite with a rise in pressure is due to the greater difficulty in the formation and migration of vacancies at higher pressures.

4.2. Influence of Oxygen Fugacity on Electrical Conductivity

During our experiments we chose three different oxygen buffers in order to explore the influence of oxygen fugacity on the electrical conductivity of Fe-bearing eclogite. For each given solid buffer, the value of the corresponding oxygen fugacity is a function of temperature and pressure; i.e., $\mathrm{Log}_{10} f_{O_2} = -\frac{a}{T} + b + c\frac{(P-1)}{T}$ (here, a, b and c are constants directly related to the standard enthalpy, the standard entropy, and the molar volume variation of the solid assemblage before and after the balancing buffer reaction, respectively; T is absolute temperature (K); and P is pressure (atm)) [*Li et al.*, 1998, 1999; *Dai et al.*, 2009]. For the three selected oxygen buffers of Cu + CuO, Ni + NiO, and Mo + MoO_2, and in that order, the values of oxygen fugacity became smaller under a wide range of temperatures from 873 to 1173 K and at a pressure of 2.0 GPa.

Figure 8 depicts the relationships between electrical conductivity and oxygen fugacity at 2.0 GPa, and with oxygen partial pressures controlled by the three solid oxygen buffers. As the oxygen fugacity rose with the sequence from Mo + MoO_2, Ni + NiO, to Cu + CuO, the electrical conductivity of the eclogite increased, and the logarithm of the preexponential factor increased from 1.32 to 1.60; at the same time, the activation enthalpy decreased from 0.86 eV to 0.81 eV. At 2.0 GPa, a quantitative and functional relationship between the electrical conductivity of eclogite and the variation of oxygen fugacity can be described as

$$\mathrm{Log}_{10}\sigma = (1.10 \pm 0.06) + i \times \mathrm{Log}_{10} f_{O_2} + \left(\frac{-3092 \pm 70}{T}\right) \quad (5)$$

At each temperature point from 873 K to 1173 K, according to the Arrhenius relation of equation (2), we can fit the exponential factor (i) for the dependence of electrical conductivity of eclogite on oxygen fugacity, and they are listed in Table 3. The value of the exponential factor increases with increasing temperature. On average, the oxygen fugacity exponent (i) is 0.048 ± 0.002.

The observed values of the exponential factors (average $i = 0.048$) are similar to those obtained previously for anhydrous Fe-bearing silicate minerals and rocks in the upper mantle and mantle transition zone. Values of 0.143–0.182 were obtained by *Duba and Constable* [1993], *Roberts and Tyburczy* [1993], and *Constable and Roberts* [1997] for anhydrous lherzolite, dunite, and olivine under conditions of room pressure and temperatures of 1173–1473 K, and with the oxygen fugacity controlled by a continuous variation in the

Table 2. Fitted Parameters of the Arrhenius Relation for the Electrical Conductivity of Eclogite

Run No.	P (GPa)	T (K)	Oxygen Buffers	Log A	ΔH (eV)	γ^2	ΔU (eV)	ΔH (cm^3/mol)
DL1503	1.0	873–1173	Cu+CuO	1.83 ± 0.11	0.84	99.38	0.86 ± 0.12	−2.51 ±0.29
DL1508	2.0	873–1173	Cu+CuO	1.60 ± 0.11	0.81	99.78		
DL1515	3.0	873–1173	Cu+CuO	1.44 ± 0.09	0.79	99.54		
DL1514	2.0	873–1173	Ni+NiO	1.43 ± 0.08	0.82	99.25	–	–
DL1506	2.0	873–1173	Mo+MoO_2	1.32 ± 0.08	0.86	99.49	–	–

Table 3. Fitted Exponential Parameters (*i*) for Eclogite Under Conditions of 2.0 GPa, 973–1173 K, With Oxygen Buffers Cu + Cu, Ni + NiO, and Mo + MoO_2, and Using Nonlinear Global Fitting of the Data

T (K)	*i*
873	0.042 ± 0.001
923	0.043 ± 0.002
973	0.046 ± 0.001
1023	0.050 ± 0.001
1073	0.053 ± 0.003
1123	0.054 ± 0.002
1173	0.055 ± 0.001
On average	0.048 ± 0.005

proportion of $CO + CO_2$ in a gas buffer across the sample cavity. A value of 0.050 was obtained by *Dai and Karato* [2009b] for anhydrous wadsleyite under a pressure of 15 GPa and temperatures of 873–1473 K, and with oxygen fugacity controlled by three solid buffers ($Mo + MoO_2$, $Ni + NiO$, and $Re + ReO_2$). In addition, values of 0.096, 0.061, and 0.054 were obtained by Dai et al. [2010, 2012, 2013] for anhydrous olivine, and pyrope-rich and almandine-rich garnet under pressures of 1–4 GPa and temperatures of 873–1423 K, and with oxygen fugacity controlled by five solid buffers ($Fe_3O_4 + Fe_2O_3$, $Ni + NiO$, $Fe + Fe_3O_4$, $Fe + FeO$, and $Mo + MoO_2$). By virtue of the similarities to the theoretical model involving concentrations of the Fe-related point defects under various chemically neutral conditions for wadsleyite [*Dai and Karato*, 2009b], we can reasonably explain the dependence of electrical conductivity on oxygen fugacity for eclogite at high temperatures and pressures.

4.3. Comparisons With Previous Studies

When considering our new results for the influence of pressure on the electrical conductivity of eclogite, we compared our data with those from previous studies [e.g., *Laštovičková and Parchomenko*, 1976; *Čermák and Laštovičková*, 1987; *Bagdassarov et al*., 2011], as shown in Figure 9. It is clear that our results plot in a higher position than other data, and some discrepancies exist between the earlier data and ours. As noted by *Karato and Dai* [2009] and *Karato* [2015], the discrepancies may be due to the different measurement methods, and it is possible that systematic errors in the calculations on the electrical conductivity of eclogite for DC and single-frequency AC technique reported by *Laštovičková and Parchomenko* [1976] have produced the discrepancies. We note that *Laštovičková and Parchomenko* [1976] found their results for the electrical conductivity of eclogite to be influenced significantly by symplectites (e.g., intergrowths of amphibole and plagioclase or diopside and plagioclase), yet it is not possible to confirm this due to the lack of any relative conductivity data. *Čermák and Laštovičková* [1987] reported electrical conductivities for eclogite at room pressure and high temperatures, and it is therefore inevitable that their conductivity results were affected by porosity and microfractures. The effect of temperature on the electrical conductivity of the At-Bashi eclogite was investigated through the impedance spectroscopy by *Bagdassarov et al.* [2011] at a pressure of 2.5 GPa and with a $Mo + MoO_2$ solid buffer, and their activation enthalpy (~0.8 eV) falls in the range of our results (0.79~0.86 eV). After we corrected for the effects of pressure and oxygen fugacity on electrical conductivity, our results are in good agreement with the electrical conductivity data for the At-Bashi

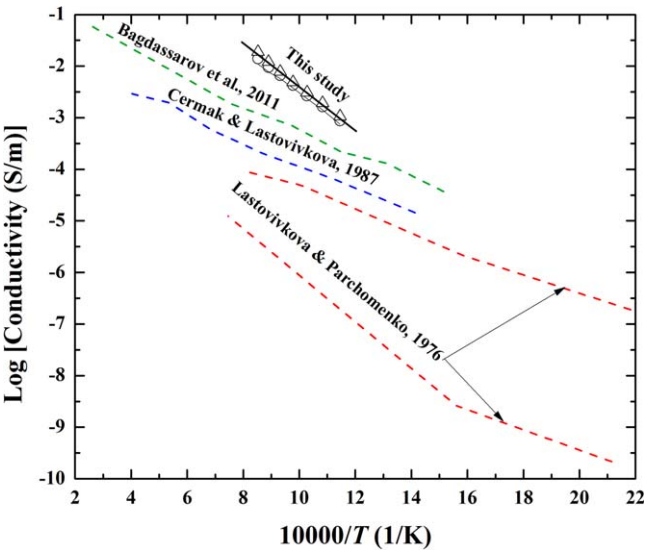

Figure 9. Comparison of the present results at pressures of 1.0–3.0 GPa (black solid lines) with previous results for the electrical conductivities of eclogite. The dashed red and blue lines represent the electrical conductivities of eclogite at pressures of 2.0–2.5 GPa from *Laštovičková and Parchomenko* [1976] and *Bagdassarov et al*. [2011], respectively, and the green broken line represents the electrical conductivity of eclogite at room pressure, from *Čermák and Laštovičková* [1987]. In considerations of differences of iron content in garnet (Fe content and its average composition for our Dabie-Sulu sample are 31.66% and ~$Alm_{70.7}Grs_{19.8}Py_{7.4}Sps_{2.1}$, respectively; Fe content and its average composition from Bagdassarov's At-Bashi sample are 27.14% and ~$Alm_{58.1}Grs_{24.0}Py_{16.0}Sps_{1.9}$) and the close Fe content in omphacite (our Dabie-Sulu sample is 4.36%; Bagdassarov At-Bashi sample is 4.54%), we found that the distinction of Fe content in garnet for dry eclogite are most possible ingredient causing the feeble conductivity discrepancy between Bagdassarov's At-Bashi sample and ours.

eclogite. As pointed out by *Bagdassarov et al*. [2011], the mineralogical content and the corresponding H_2O partition coefficient for garnet and omphacite in hydrous eclogite are two best candidate factors that may result in differences of electrical conductivity. And furthermore, in considerations of differences of iron content in garnet (Fe content and its average composition for our Dabie-Sulu sample are 31.66% and $\sim Alm_{70.7}Grs_{19.8}Py_{7.4}Sps_{2.1}$, respectively; Fe content and its average composition from Bagdassarov's At-Bashi sample are 27.14% and $\sim Alm_{58.1}Grs_{24.0}Py_{16.0}Sps_{1.9}$) and the close Fe content in omphacite (our Dabie-Sulu sample is 4.36%; Bagdassarov's At-Bashi sample is 4.54%), we found that the distinction of Fe content in garnet for dry eclogite are most possible ingredient causing the feeble conductivity discrepancy between Bagdassarov's At-Bashi sample and ours. A compositionally complex and heterogeneous rock sample may produce conductivity discrepancies owing to the comprehensive effects of various water contents, iron contents, mineralogical composition, and redox environments, all of which may be relevant when conducting conductivity measurements in a variety of environments, and there could possibly be several magnitudes of variation in the measured electrical conductivities of eclogite. Unfortunately, in previous studies the influences of these various factors on the measurements of electrical conductivity have not generally been quantified.

4.4. Conduction Mechanisms

A fundamental expression describing the specific conductivity of a silicate mineral and a rock for each charge carrier (or defect) species is given by

$$\sigma = \sum_j q_j N_j \mu_j \tag{6}$$

where q_j is the effective charge ($q = ze$), N_j is the concentration of point defects for the j-th species, and μ_j is the mobility ($\mu_j = v/E$, where v is the drift velocity of the particle and E is the applied electric field). In light of the dependence of the activation enthalpy for each conduction mechanism on charge-carrier mobility, every conduction mechanism can be distinguished by a different slope (activation enthalpy), as defined in a specific temperature region of the Arrhenius diagram. In the case of our new data for eclogite, the Arrhenius plot displays only a linear relationship between the logarithm of electrical conductivity and temperature, which suggests that only one conduction mechanism can be identified.

The conduction mechanism of the hopping of small polarons between ferrous and ferric iron is characterized by low values of activation enthalpy (<2.0 eV) and a negative activation volume (i.e., the electrical conductivity decreased with increasing pressure) due to the greater difficulty in the formation and migration of vacancies at high pressures [*Goddat et al*., 1999; *Ono and Mibe*, 2015]. Our results give values for the activation enthalpy in the range 0.79–0.86 eV, and the activation volume is negative (-2.51 cm^3/mole), and therefore the hopping of small polarons can make a significant contribution to the electrical conductivity of eclogite at high temperatures and pressures, and with varying oxygen fugacities. A small polaron is formed according to the following point defect reaction [*Schock et al*., 1989; *Hirsch et al*., 1993; *Dai and Karato*, 2014a],

$$Fe^{\times}_{Mg} + h^{\bullet} \rightleftharpoons Fe^{\bullet}_{Mg} \tag{7}$$

where $Fe^{\times}_{Mg}$ and $Fe^{\bullet}_{Mg}$ are respectively the ferrous and ferric ions on the site of the magnesium ion in the lattice. The dominant charge carrier is the small polaron, $Fe^{\bullet}_{Mg}$ (Fe^{3+} at Mg site). These small polarons contribute conduction via the hopping of holes ($h^{\bullet}$) between $Fe^{\times}_{Mg}$ and $Fe^{\bullet}_{Mg}$. In addition, the observed exponential factors (average $q = 0.048$) for the dependence of the electrical conductivity of eclogite on oxygen fugacity are similar to those of anhydrous Fe-bearing silicate minerals and rocks where the migration of iron-related defects (small polarons) occurs. Because the electrical conductivity of eclogite shows a positive correlation with the concentration of point defects, a higher concentration of small polarons will be produced as a result of the point defect reactions, and thus the electrical conductivity increases with increasing in oxygen fugacity.

On the other hand, other conduction mechanisms such as hydrogen-related defects and ion conduction are unlikely to play an important role in the electrical conductivity of eclogite at high pressures. Proton conduction is considered an important mechanism if the nominally anhydrous minerals and rocks contain a certain amount of structural water [*Yoshino et al*., 2006, 2008; *Yoshino and Katsura*, 2013; *Dai and Karato*,

2014a, 2014b, 2014c, 2014d, 2015; *Dai et al*., 2015a]. Although the experimentally obtained values of less than 1.0 eV for the activation enthalpy of hydrous orthopyroxene [*Dai and Karato*, 2009c], garnet [*Dai and Karato*, 2009a; *Dai et al*., 2012], and olivine and its high-pressure polymorphs [*Huang et al*., 2005; *Dai and Karato*, 2014c] are very close to our results for eclogite, the negative dependence of electrical conductivity on oxygen fugacity has been confirmed for hydrous olivine, wadsleyite, garnet, and gabbro by *Dai and Karato* [2009b,d] and *Dai et al*. [2012, 2015b]. In addition, another three potential substituent hydrogen-related defect species ($(2H)^{\times}_{Me}$ (two protons in Me-site vacancies), $(4H)^{\times}_{Si}$ (four protons at Si site vacancies) and H_i (interstitial protons)) were recognized by the study of the inferring electrical conductivity results from diffusion calculation and directly measuring the anisotropic electrical conductivity along three different crystallographic axis of hydrous single crystal olivine [*Demouchy and Mackwell*, 2006; *Kohlstedt*, 2006; *Ingrin et al*., 2013]. However, as pointed out by *Gardés et al*. [2014, 2015], they are more inclined to be rather electronic than the conduction mechanism of hydrogen-related defects. With regard to ion conduction, it has been proposed as one of the main conduction mechanisms in many anhydrous silicate and carbonate minerals, such as Mg-perovskite, aragonite, and anorthite [*Xu and McCammon*, 2002; *Dobson*, 2003; *Ono and Mibe*, 2013; *Hu et al*., 2015]. All of these obtained results has confirmed that the ion conduction mechanism is characterized by an activation enthalpy that is higher than 2.0 eV and a positive activation volume. We conclude, therefore, that our data for Fe-bearing eclogites, including the negative activation volume (-2.51 cm^3/mole), the lower activation enthalpy (0.79–0.86 eV), and the positive relationship of the dependency of electrical conductivity on oxygen fugacity (0.050), rule out any significant contributions from the proton and ion conduction mechanisms. Small polarons are the best candidates for charge carriers in eclogite, and they hop between the ferrous and ferric ions on the site of the magnesium ion in the lattice.

5. Geophysical Implications

Eclogites that are formed during a regional metamorphism under conditions of high or ultrahigh pressures and temperatures, usually coexist with granulite-facies rocks. Together with the granulite, the eclogite can be used to explain the high-conductivity anomalies in the deep crust of the Earth, especially in the ultra-high pressure metamorphic (UHPM) belts such as those of Dabie-Sulu terrane and the southern Tibet. Therefore, on the basis of the average heat flow values from three models of geothermal gradients in stable continental crust (60 mW/m^2) and the Dabie-Sulu terrane (the heat flows results of 24 mW/m^2 and 75 mW/m^2 corresponds to the lower and upper boundary in the Sulu-Dabie UHPM belts, respectively) [*Taylor and McLennan*, 1995; *He et al*., 2009], two sets of correspondent laboratory-based conductivity-depth profiles can be constructed by converting the conductivity-temperature data into conductivity-depth results, in combination with all the parameters we determined with the Arrhenius relation 2 under a pressure of 2.0 GPa, and with three different controls on oxygen fugacities (Cu + CuO, Ni + NiO, and Mo + MoO_2). The influence of pressure on the electrical conductivity of eclogite is minor, and we can therefore ignore it. A similar transformation from the result on electrical conductivity of granulite by *Fuji-ta et al*. [2004] at a pressure of 1.0 GPa and with an oxygen fugacity controlled by the Mo + MoO_2 buffer has been conducted. Meantime, we also made comparisons for granulite and eclogite with the magnetotelluric conductivity results for the anomalous high-conductivity zone (HCZ; conductivity values of 10^{-2} to 10^{-1} S/m) that exists under stable midlower continental crust at depths of 20–30 km [*Glover and Vine*, 1994; *Lemonnier et al*., 1999; *Dai et al*., 2014], and with the high electrical conductivity zone (conductivities $\geq 10^{-1}$ S/m) in the Dabie-Sulu ultra-high pressure metamorphic belts at depths of 12–21 km [*Hu et al*., 2000; *Xiao et al*., 2007; *He et al*., 2009], as shown in Figure 10.

The profiles make it clear that the electrical conductivities of eclogite in various redox environments are lower (by at least a ~1.5 logarithmic magnitude) than those of the anomalous high conductivity zones beneath the stable continental crust and Dabie-Sulu UHPM belts. In accordance with the sequence of oxygen buffers from Cu + CuO to Ni + NiO to Mo + MoO_2, the range of oxygen partial pressures during our conductivity measurements gradually moved from an oxidized to a reduced state under the same conditions of temperature and pressure. Although we have fully considered the effects of oxygen fugacity on the electrical conductivity of eclogite, our results cannot account for the high conductivity anomalies, inferred from magnetotelluric data, in the globally stable midlower continental crust, and the middle crust of the Dabie-Sulu UHPM belts. We reached a consistent conclusion obtained by *Fuji-ta et al*. [2004] for granulite at 1.0 GPa that the electrical conductivity of granulite cannot explain the available high conductivity anomalies extrapolated from MT data in the globally stable lower continental crust. However, some

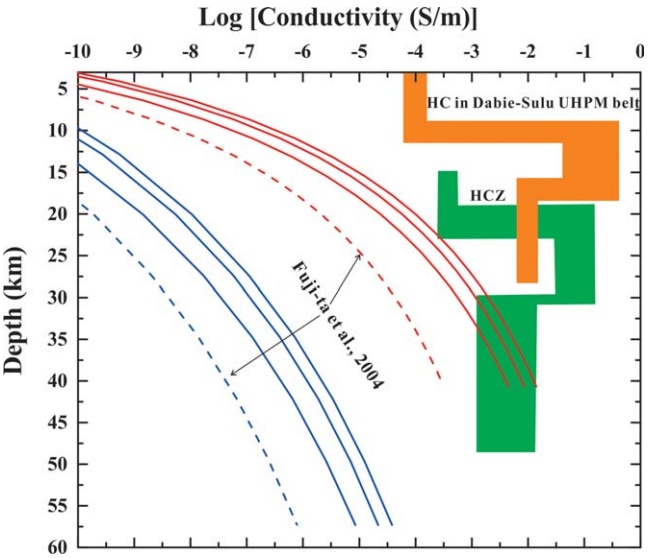

Figure 10. Two sets of laboratory-based conductivity-depth profiles as a function of different oxygen partial pressures (using Cu + CuO, Ni + NiO, and Mo + MoO_2 buffers), compared with the magnetotelluric field results for granulite and the anomalous high conductivity zones (HCZ) under the stable midlower continental crust and Dabie-Sulu UHPM belts, respectively. The solid blue and red lines indicate the laboratory-based conductivity-depth profiles for eclogite based on heat flow values of 24 and 75 mW/m^2 for the lower and upper boundary of Dabie-Sulu UHPM belts, respectively. The broken blue and red lines indicate the laboratory-based conductivity-depth profiles for granulite based on same heat flow values of 24 and 75 mW/m^2, respectively [*Fuji-ta et al.*, 2004]. The dark orange and green regions denote the high-conductivity anomalies beneath Dabie-Sulu ultrahigh-pressure metamorphic belts at depths of 12–21 km [*Hu et al.*, 2000; *Xiao et al.*, 2007; *He et al.*, 2009] and the HCZ in stable mid- to lower-continental crust at depths of 20–30 km [*Glover and Vine*, 1994], respectively.

substituent causes including hydrous fluids, brine-bearing fluids, the interconnected secondary high conductivity phases (e.g., graphite, ilmenite, magnetite and pyrite etc. along the grain boundaries of minerals), dehydration of minerals and partial melting are possible to result in the high conductivity anomalies in the deep crust [*Nover et al.*, 1998; *Nover*, 2005; *Yoshino*, 2010; *Hashim et al.*, 2013; *Selway*, 2014; *Shimojuku et al.*, 2014]. Besides, the horizontal variations in conductivity of other constituent rocks with low electrical conductivities may be another one substituent cause of a relatively low magnetotelluric result for the globally stable midlower continental crust areas [*Xie et al.*, 2004; *Mareschal and Jaupart*, 2013; *Aguilar et al.*, 2015]. Consequently, the conductivity-depth profiles we have constructed for eclogites under various redox conditions may provide important constraints on the interpretation of field magnetotelluric conductivity results for a wide range of oxidation-reduction boundaries at various depths in the interior of the Earth.

Acknowledgments
We thank the editor of Ulrich Faul and two anonymous reviewers for their very constructive and enlightened comments and suggestions in the reviewing process, which helped us greatly in improving the manuscript. Some crucial discussions in petrological background and the mass balance calculation for the whole rock composition for the Dabie-Sulu ultrahigh pressure metamorphic belts of eastern China were made with Professor Hongfeng Tang. This research was supported financially by the Strategic Priority Research Program (B) of the Chinese Academy of Sciences (XDB 18010401), the Hundred Talents program of CAS, the Youth Innovation Promotion Association of CAS, the NSF of China (41474078, 41304068, and 41174079) and the Special fund of the West Light Foundation of CAS.

References

Aguilar, C., M. Liesa, P. Štípská, K. Schulmann, J. A. Muñoz, and J. M. Casas (2015), P–T–t–d evolution of orogenic middle crust of the Roc de Frausa Massif (Eastern Pyrenees): A result of horizontal crustal flow and Carboniferous doming?, *J. Metamorph. Geol.*, *33*(3), 273–294.

Anderson, D. L. (1989), *Theory of the Earth*, pp. 129–143, Blackwell Sci., Oxford, U. K.

Bagdassarov, N., V. Batalev, and V. Egorova (2011), State of lithosphere beneath Tien Shan from petrology and electrical conductivity of xenoliths, *J. Geophys. Res.*, *116*, B01202, doi:10.1029/2009JB007125.

Burnham, A. D., and A. J. Berry (2014), The effect of oxygen fugacity, melt composition, temperature and pressure on the oxidation state of cerium in silicate melts, *Chem. Geol.*, *366*, 52–60.

Čermák, V., and M. Laštovičková (1987), Temperature profiles in the Earth of importance to deep electrical conductivity models, *Pure Appl. Geophys.*, *125*(2–3), 255–284.

Constable, S., and J. J. Roberts (1997), Simultaneous modeling of thermopower and electrical conduction in olivine, *Phys. Chem. Miner.*, *24*(5), 319–325.

Dai, L., and S.-I. Karato (2009a), Electrical conductivity of pyrope-rich garnet at high temperature and high pressure, *Phys. Earth Planet. Inter.*, *176*(1), 83–88.

Dai, L., and S.-I. Karato (2009b), Electrical conductivity of wadsleyite at high temperatures and high pressures, *Earth Planet. Sci. Lett.*, *287* (1), 277–283.

Dai, L., and S.-I. Karato (2009c), Electrical conductivity of orthopyroxene: Implications for the water content of the asthenosphere, *Proc. Jpn. Acad., Ser. B*, *85* (10), 466–475.

Dai, L., and S.-I. Karato (2014a), Influence of FeO and H on the electrical conductivity of olivine, *Phys. Earth Planet. Inter.*, *237*, 73–79.

Dai, L., and S.-I. Karato (2014b), The effect of pressure on the electrical conductivity of olivine under the hydrogen-rich conditions, *Phys. Earth Planet. Inter.*, *232*, 51–56.

Dai, L., and S.-I. Karato (2014c), High and highly anisotropic electrical conductivity of the asthenosphere due to hydrogen diffusion in olivine, *Earth Planet. Sci. Lett.*, *408*, 79–86.

Dai, L., and S.-I. Karato (2014d), Influence of oxygen fugacity on the electrical conductivity of hydrous olivine: Implications for the mechanism of conduction, *Phys. Earth Planet. Inter.*, *232*, 57–60.

Dai, L., and S.-I. Karato (2015), Reply to comment on "High and highly anisotropic electrical conductivity of the asthenosphere due to hydrogen diffusion in olivine" by Dai and Karato [Earth Planet. Sci. Lett. 408 (2014) 79–86], *Earth Planet. Sci. Lett.*, *427*, 300–302.

Dai, L., H. Li, C. Liu, S. Shan, T. Cui, and G. Su (2005), Experimental study on the electrical conductivity of orthopyroxene at high temperature and high pressure under different oxygen fugacities, *Acta Geol. Sin.*, *79* (6), 803–809.

Dai, L., H. Li, H. Hu, and S. Shan (2008), Experimental study of grain boundary electrical conductivities of dry synthetic peridotite under high-temperature, high-pressure, and different oxygen fugacity conditions, *J. Geophys. Res.*, *113*, B12211, doi: 10.1029/2008JB005820.

Dai, L., H. Li, H. Hu, and S. Shan (2009), Novel technique to control oxygen fugacity during high-pressure measurements of grain boundary conductivities of rocks, *Rev. Sci. Instrum.*, *80*, 033903, doi 10.1063/1.3097882.
Dai, L., H. Li, C. Li, H. Hu, and S. Shan (2010), The electrical conductivity of dry polycrystalline olivine compacts at high temperatures and pressures, *Mineral. Mag.*, *74* (5), 849–857.
Dai, L., H. Li, H. Hu, S. Shan, J. Jiang, and K. Hui (2012), The effect of chemical composition and oxygen fugacity on the electrical conductivity of dry and hydrous garnet at high temperatures and pressures, *Contrib. Mineral. Petrol.*, *163*(4), 689–700.
Dai, L., H. Li, H. Hu, J. Jiang, K. Hui, and S. Shan (2013), Electrical conductivity of $Alm_{82}Py_{15}Grs_3$ almandine-rich garnet determined by impedance spectroscopy at high temperatures and high pressures, *Tectonophysics*, *608*, 1086–1093.
Dai, L., H. Hu, H. Li, J. Jiang, and K. Hui (2014), Influence of temperature, pressure, and chemical composition on the electrical conductivity of granite, *Am. Mineral.*, *99* (7), 1420–1428.
Dai, L., J. Jiang, H. Li, H. Hu, and K. Hui (2015a), Electrical conductivity of hydrous natural basalts at high temperatures and pressures, *J. Appl. Geophys.*, *112*, 290–297.
Dai, L., H. Hu, H. Li, K. Hui, J. Jiang, J. Li, and W. Sun (2015b), Electrical conductivity of gabbro: The effects of temperature, pressure and oxygen fugacity, *Eur. J. Mineral.*, *27*, 215–224.
Demouchy, S., and S. J. Mackwell (2006), Mechanisms of hydrogen incorporation and diffusion in iron-bearing olivine, *Phys. Chem. Miner.*, *33*, 347–355.
Dobson, D. (2003), Oxygen ionic conduction in $MgSiO_3$ perovskite, *Phys. Earth Planet. Inter.*, *139* (1), 55–64.
Duba, A., and S. Constable (1993), The electrical conductivity of lherzolite, *J. Geophys. Res.*, *98*, 11,885–11,899.
Du Frane, W. L., J. J. Roberts, D. A. Toffelmier, and J. A. Tyburczy (2005), Anisotropy of electrical conductivity in dry olivine, *Geophys. Res. Lett.*, *32*, L24315, doi:10.1029/2005GL023879.
Fuji-ta, K., T. Katsura, and Y. Tainosho (2004), Electrical conductivity measurement of granulite under mid-to lower crustal pressure-temperature conditions, *Geophys. J. Int.*, *157*(1), 79–86.
Gaillard, F. (2004), Laboratory measurements of electrical conductivity of hydrous and dry silicic melts under pressure, *Earth Planet. Sci. Lett.*, *218*, 215–228.
Gaillard, F., B. Scaillet, M. Pichavant, and G. Iacono-Marziano (2015), The redox geodynamics linking basalts and their mantle sources through space and time, *Chem. Geol.*, *418*, 217–233.
Gardés, E., F. Gaillard, and P. Tarits (2014), Toward a unified hydrous olivine electrical conductivity law, *Geochem. Geophys. Geosyst.*, *15*, 4984–5000, doi:10.1002/2014GC005496.
Gardés, E., F. Gaillard, and P. Tarits (2015), Comment to "High and highly anisotropic electrical conductivity of the asthenosphere due to hydrogen diffusion in olivine" by Dai and Karato [Earth Planet. Sci. Lett. 408 (2014) 79–86], *Earth Planet. Sci. Lett.*, *427*, 296–299.
Glover, P. W., and F. J. Vine (1994), Electrical conductivity of the continental crust, *Geophys. Res. Lett.*, *21*, 2357–2360.
Goddat, A., J. Peyronneau, and J. P. Poirier (1999), Dependence on pressure of conduction by hopping of small polarons in minerals of the Earth's lower mantle, *Phys. Chem. Miner.*, *27*(2), 81–87.
Hashim, L., F. Gaillard, R. Champallier, N. Le Breton, L. Arbaret, and B. Scaillet (2013), Experimental assessment of the relationships between electrical resistivity, crustal melting and strain localization beneath the Himalayan–Tibetan Belt, *Earth Planet. Sci. Lett.*, *373*, 20–30.
He, L., S. Hu, W. Yang, and J. Wang (2009), Radiogenic heat production in the lithosphere of Sulu ultrahigh-pressure metamorphic belt, Earth Planet. Sci. Lett., *277*(3), 525–538.
Hirsch, L. M., T. J. Shankland, and A. G. Duba (1993), Electrical conduction and polaron mobility in Fe-bearing olivine, *Geophys. J. Int.*, *114* (1), 36–44.
Hu, H., H. Li, L. Dai, S. Shan, and C. Zhu (2011), Electrical conductivity of albite at high temperatures and high pressures, *Am. Mineral.*, *96*(11–12), 1821–1827.
Hu, H., L. Dai, H. Li, K. Hui, and J. Li (2015), Temperature and pressure dependence of electrical conductivity in synthetic anorthite, *Solid State Ionics*, *276*, 136–141.
Hu, S., L. He, and J. Wang (2000), Heat flow in the continental area of China: A new data set, *Earth Planet. Sci. Lett.*, *179*(2), 407–419.
Huang, X., Y. Xu, and S.-I. Karato (2005), Water content in the transition zone from electrical conductivity of wadsleyite and ringwoodite, *Nature*, *434*(7034), 746–749.
Huebner, J. S., and D. E. Voigt (1988), *Electrical conductivity of diopside: Evidence for oxygen vacancies, Am*. Mineral., 73(11–12), 1235–1254.
Ingrin, J., J. Liu, C. Depecker, S. C. Kohn, E. Balan, and K. J. Grant (2013), Low-temperature evolution of OH bands in synthetic forsterite, implication for the nature of H defects at high pressure, *Phys. Chem. Miner.*, *40*, 499–510.
Karato, S.-I. (2013), Theory of isotope diffusion in a material with multiple species and its implications for hydrogen-enhanced electrical conductivity in olivine, *Phys. Earth Planet. Inter.*, *219*, 49–54.
Karato, S.-I. (2015), Some notes on hydrogen-related point defects and their role in the isotope exchange and electrical conductivity in olivine, *Phys. Earth Planet. Inter.*, *248*, 94–98.
Karato, S.-I., and L. Dai (2009), Comments on "Electrical conductivity of wadsleyite as a function of temperature and water content" by Manthilake et al., *Phys. Earth Planet. Inter.*, *174* (1), 19–21.
Keyes, R.W. (1963), Continuum models of the effect of pressure on activated processes, in *Solids Under Pressure*, edited by W. Paul and D. M. Warschauer, pp. 71–100, McGraw-Hill, N. Y.
Knipping, J. L., H. Behrens, M. Wilke, J. Goettlicher, and P. Stabile (2015), Effect of oxygen fugacity on the coordination and oxidation state of iron in alkali bearing silicate melts, *Chem. Geol.*, *411*, 143–154.
Kohlstedt, D. L. (2006), The role of water in high-temperature rock deformation, *Rev. Mineral. Geochem.*, *62*, 377–396.
Laštovičková, M., and E. I. Parchomenko (1976), The electric properties of eclogites from the Bohemian Massif under high temperatures and pressures, *Pure Appl. Geophys.*, *114*(3), 451–460.
Lemonnier, C., G. Marquis, F. Perrier, J. P. Avouac, G. Chitrakar, B. Kafle, S. Sapkota, U. Gautam, D. Tiwari, and M. Bano (1999), Electrical structure of the Himalaya of central Nepal: High conductivity around the mid-crustal ramp along the MHT, *Geophys. Res. Lett.*, *26*, 3261–3264.
Li, H., H. Xie, J. Guo, Y. Zhang, Z. Xu, and J. A. Xu (1998), In situ control of oxygen fugacity at high temperature and high pressure: A Ni–O system, *Geophys. Res. Lett.*, *25*, 817–820.
Li, H., H. Xie, J. Guo, Y. Zhang, Z. Xu, and C. Liu (1999), In situ control of oxygen fugacity at high temperature and high pressure, *J. Geophys. Res.*, *104*, 29,439–29,451.
Mareschal, J. C., and C. Jaupart (2013), Radiogenic heat production, thermal regime and evolution of continental crust, *Tectonophysics*, *609*, 524–534.
Nishihara, Y., T. Shinmei, and S.-I. Karato (2008), Effect of chemical environment on the hydrogen-related defect chemistry in wadsleyite, *Am. Mineral.*, *93*(5–6), 831–843.

Nover, G. (2005), Electrical properties of crustal and mantle rocks–a review of laboratory measurements and their explanation, *Surv. Geophys.*, *26*(5), 593–651.
Nover, G., G. Will, and R. Waitz (1992), Pressure induced phase transition in Mg_2GeO_4 as determined by frequency dependent complex electrical resistivity measurements, *Phys. Chem. Miner.*, *19*(3), 133–139.
Nover, G., S. Heikamp, H. J. Meurer, and D. Freund (1998), In-situ electrical conductivity and permeability of mid-crustal rocks from the KTB drilling: Consequences for high conductive layers in the earth crust, *Surv. Geophys.*, *19*(1), 73–85.
Ono, S., and K. Mibe (2013), Electrical conductivity of aragonite in the subducted slab, *Eur. J. Mineral.*, *25*(1), 11–15.
Ono, S., and K. Mibe (2015), Influence of pressure and temperature on the electrical conductivity of dolomite, *Phys. Chem. Miner.*, *42*(9), 773–779.
Paterson, M. S. (1982), The determination of hydroxyl by infrared absorption in quartz, silicate glasses, and similar materials, *Bull. Mineral.*, *105*, 20–29.
Pommier, A., F. Gaillard, and M. Pichavant (2010), Time-dependent changes of the electrical conductivity of basaltic melts with redox state, *Geochim. Cosmochim. Acta*, *74*, 1653–1671.
Roberts, J. J. (2002), Electrical properties of microporous rock as a function of saturation and temperature, *J. Appl. Phys.*, *91*(3), 1687–1694.
Roberts, J. J., and A. G. Duba (1995), Transient electrical response of San Quintin dunite as a function of oxygen fugacity changes: Information about charge carriers, *Geophys. Res. Lett.*, *22*, 453–456.
Roberts, J. J., and J. A. Tyburczy (1991), Frequency dependent electrical properties of polycrystalline olivine compacts, *J. Geophys. Res.*, *96*, 16,205–16,222.
Roberts, J. J., and J. A. Tyburczy (1993), Frequency dependent electrical properties of dunite as functions of temperature and oxygen fugacity, *Phys. Chem. Miner.*, *19*(8), 545–561.
Roberts, J. J., and J. A. Tyburczy (1994), Frequency dependent electrical properties of minerals and partial–melts, *Surv. Geophys.*, *15*(2), 239–262.
Romano, C., B. T. Poe, N. Kreidie, and C. A. McCammon (2006), Electrical conductivities of pyrope-almandine garnets up to 19 GPa and 1700 °C, *Am. Mineral.*, *91*(8–9), 1371–1377.
Schock, R. N., A. G. Duba, and T. J. Shankland (1989), Electrical conduction in olivine, *J. Geophys. Res.*, *94*, 5829–5839.
Selway, K. (2014), On the causes of electrical conductivity anomalies in tectonically stable lithosphere, *Surv. Geophys.*, *35*(1), 219–257.
Shimojuku, A., T. Yoshino, and D. Yamazaki (2014), Electrical conductivity of brine-bearing quartzite at 1 GPa: Implications for fluid content and salinity of the crust, *Earth Planets Space, 2014*, *66*(2), 1–9.
Tang, H. F., C. Q. Liu, S. I. Nakai, and Y. Orihashi (2007), Geochemistry of eclogites from the Dabie–Sulu terrane, eastern China: New insights into protoliths and trace element behaviour during UHP metamorphism, *Lithos*, *95*(3), 441–457.
Taylor, S. R., and S. M. McLennan (1995), The geochemical evolution of the continental crust, *Rev. Geophys.*, *33*, 241–265.
Wanamaker, B. J. (1994), Point defect diffusivites in San Carlos olivine derived from reequilibration of electrical conductivity following changes in oxygen fugacity, *Geophys. Res. Lett.*, *21*, 21–24.
Xiao, Q. B., G. Z. Zhao, Y. Zhan, X. B. Chen, J. Tang, J. J. Wang, and Deng, Q. H (2007), A preliminary study on electrical structure and dynamics of the ultra-high pressure metamorphic belt beneath the Dabie Mountains, *Chin. J. Geophys.*, *50*(3), 710–721.
Xie, J., R. Gok, J. Ni, and Y. Aoki (2004), Lateral variations of crustal seismic attenuation along the INDEPTH profiles in Tibet from Lg Q inversion, *J. Geophys. Res.*, *109*, B10308, doi:10.1029/2004JB002988.
Xu, Y., and C. McCammon (2002), Evidence for ionic conductivity in lower mantle (Mg,Fe)(Si,Al)O_3 perovskite, *J. Geophys. Res.*, *107*(B10), 2251, doi:10.1029/2001JB000677.
Xu, Y., T. J. Shankland., and A. G. Duba (2000), Pressure effect on electrical conductivity of mantle olivine, *Phys. Earth Planet. Inter.*, *118*(1), 149–161.
Yoshino, T. (2010), Laboratory electrical conductivity measurement of mantle minerals, *Surv. Geophys.*, *31*(2), 163–206.
Yoshino, T., and T. Katsura (2013), Electrical conductivity of mantle minerals: Role of water in conductivity anomalies, *Annu. Rev. Earth Planet. Sci.*, *41*, 605–628.
Yoshino, T., T. Matsuzaki, S. Yamashita, and T. Katsura (2006), Hydrous olivine unable to account for conductivity anomaly at the top of the asthenosphere, *Nature*, *443*, 973–976.
Yoshino, T., G. Manthilake, T. Matsuzaki, and T. Katsura (2008), Dry mantle transition zone inferred from the conductivity of wadsleyite and ringwoodite, *Nature*, *451*, 326–329.
Zheng, Y. F., B. Fu, B. Gong, and L. Li (2003), Stable isotope geochemistry of ultrahigh pressure metamorphic rocks from the Dabie-Sulu orogen in China: Implications for geodynamics and fluid regime, *Earth Sci. Rev.*, *62*(1), 105–161.